Flexural and Tensile Performance of Laminated GFRP as Suitable Alternative to Hydraulic Steel Gates

B.H. MOHAMED [1]
A.M. ANWAR[2]
H.H. ELTOBGY[3]
G. HELMY[4]

Abstract: Hydraulic steel gates are commonly used for their superior characteristics in carrying both tensile and compressive stresses. Corrosion, operation, and maintenance costs make it essential to search for suitable alternatives. In this research, Glass Fiber Reinforced Polymers (GFRP) were investigated as a promising choice that can be used to resist flexure stresses as in case of hydraulic gates. Firstly, typical mechanical tests were conducted on nine specimens made of pure steel beams, four ribbed steel beams, twenty-four specimens of pure GFRP beams, along with four combined specimens from both materials. GFRP beams were also used in cooperation with polyester cemented sand to form a sandwich like beam. It was concluded that beams from GFRP achieved similar flexural capacity of steel beams of slimmer thickness. Combinations of steel and GFRP show satisfactory results while maintaining member ductility. The load capacity of the strengthened steel beams increased by 80% to 97% compared to specimens made from steel only. Failure modes for all specimens were introduced and compared. Moreover, numerical investigation was conducted using ABAQUS nonlinear module. Finite element models for three small gates of dimensions (1.0 x 1.0 m). A steel gate of thickness 14mm, Pure GFRP gates of thicknesses 29mm and 45mm were simulated. The 29mm GFRP gate was able to bear almost the same loads of the steel gate with equivalent deflection. Finally, it can be concluded that for small-scale hydraulic gates, GFRP can effectively be used as a suitable alternative for steel gates after setting limitations for failure strains.

1. Introduction

Worldwide, the production of steel has become expensive due to the global increase in iron ore price. Additionally, steel is characterized by its high toughness, tensile, and compressive

¹ Assist. Researcher, Construction Research Institute, National Water Research Center, Egypt. basma_elbably@nwrc.gov.eg
² Assoc., Professor, Construction Research Institute, National Water Research Center, Egypt. ahmed_anwar@nwrc.gov.eg
³ Assoc. Professor, Dept. of Civil. Eng., Benha University-Shoubra, Egypt. hanan.altobgy@feng.bu.edu.eg
⁴ Professor, Dept. of Civil. Eng., Benha University-Shoubra, Egypt. gelsaeed@feng.bu.edu.eg

strength [1]. On the other hand, steel has a big unit mass with a high probability of corrosion and deterioration if not well protected. Hydraulic gates are often subjected to harsh environments that require intensive periodical monitoring and maintenance programs [2] & [3]. Hydraulic gates can be found in large scale sizes such as miter gates, tainter gates, lift gates, and stoplogs [4]. Hydraulic gates can also be used to control the flow of water in small intakes and culverts. In the current research, an attempt to replace/strengthen small scale steel gates by GFRP was conducted. The use of GFRP could act as a suitable alternative to steel where it is environmentally friendly, relatively low cost and exerted good strength.

Recently, Fiber-reinforced polymers (FRP) have been widely involved in a lot of applications [5]. There are already over 400 FRP gates serving in Japan [6]. A numerical study was applied to the design of a radial gate with different materials including fibers. This research resulted in having a light weight, economical polymer gate that can be operated with minimum effort [7]. Moreover, experimental and numerical studies were performed in a wicket gate under water pressure in closed and opened scenarios; the study assured the success of the FRP wicket gate in bearing hydrostatic loads [8]. The usage of GFRP instead of steel was nominated because of corrosion, fabrications, and maintenance cost [9]. FRP can be commercially found in the form of sheets, laminates, and rods. High strength, durability, high modulus of elasticity, no corrosion attack, light mass… etc., are among the advantages of using FRP products. Fiber can be glass, carbon, and aramid. They are embedded in a resin matrix that bonds together and gives them additional protection [10]. Many researchers conducted a lot of studies on fibers and their uses [11]. Most probably, FRPs are widely used for external strengthening purposes such as strengthening reinforced concrete and steel structures [12]. Also, to enhance the torsional behavior of the concrete beams [13]. FRPs can be used for their high stiffness, and strength, and at the same time did not change the structure dimensions or mass [14] & [15]. GFRP was used to reinforce cold-formed steel members to increase their load-carrying capacity up to 40% [16]. It was also used to reinforce various conventional steel structures like columns and beams and unconventional steel structures like marines and hydraulic gates, as it gave a boost of strength over the strength of the original beam, enhanced the static and dynamic behavior, and delayed the formation of local buckling [17]. FRP rods can be used as structure members instead of steel bars in the concrete members [18] and they give good resistance to corrosion and enhance the flexure behavior of concrete structures. Another promising benefit of using FRP is to be utilized in the manufacturing of the honeycomb sandwich structures that are used in aerospace structures, and automotive industries as well as for rehabilitation purposes [19].

However, creep is considered a weak point in the use of GFRP application. According to ASTM-D2990-09 [20] the creep rapture phenomenon is the calculated time to fail under constant load. Creep cure consists of three stages: primary, secondary, and tertiary; the first stage represents the zone of the elastic strain where the creep rate decreases rapidly. In the second stage, it reached the steady state zone. In the third level it reached the maximum value of the creep, and the failure occurs. Silvestre N. et al. [21] carried out flexure creep test on small specimens of GFRP to sustain stress up to 20% and 80 % of the ultimate stress,

the deflection was measured after 1600 hours, and the results assured that small specimens were capable to indicate creep of GFRP constructions. Loni et al. [22] conducted a four-point flexure test on GFRP beams to describe the creep behavior in the short and long term at different controlled temperatures with different load percentages. Additionally, Beddu [23] used finite element models to study the effect of creep among GFRP. It was also stated that a reduction in Young's Modulus occurred after 14 months while reduction in shear modulus was assumed 43% after fifty years. Thus, creep effects should not be ignored for GFRP applications.

The research started with an attempt to check the adequacy of using GFRP alone or combined with steel sections in small scale beams. GFRP was used to form controlled handmade laminates that were used to resist flexural stresses. Glass fibers were used in the form of chopped and woven roving mats. Polyester was chosen as a binding material. The formed layers were utilized through wet application procedure to form strong laminates of GFRP. Tensile tests were conducted on GFRP coupons with different thicknesses to ensure their effectiveness and behavior till failure. Moreover, beams of different configurations were also examined and compared with steel sections. On the other hand, built-up ribbed steel sections were also investigated as a trail to sustain higher stresses with lighter sections. Alternatively, ribbed GFRP sections infilled with cemented sand were also introduced and examined. Results and observations for all steel and GFRP samples are introduced as well as their modes of failure. In the light of the results, the specimens' size was enlarged, and prototype gates were examined numerically.

2. Materials and Methods

2.1. Steel Plates
In the current study, commercially certified steel grades (St 52) were used as per the Egyptian Code of Practice for Steel Construction and Bridges, Allowable Stress Design (ASD) [24]. The steel's ultimate strength, yield stress, and modulus of elasticity were 520, 360, and 210000 MPa. Steel was used in the form of thin coupons for tensile strength tests and in the form of beams of variable thicknesses for flexure. In addition, built-up ribbed beams were also considered as an attempt to achieve higher flexural rigidity with minimal cost.

2.2. Glass Fiber Reinforced Polymers (GFRP)
In this study, Glass Fiber Reinforced Polymers (GFRP) are used as they have high strength, good water resistance, good electrical insulation properties, good durability properties, and corrosion resistance [2] & [25]. A single layer of GFRP laminate was prepared as follows: a layer of woven roving combined with a layer of chopped mate squeezed together using high polyester resin. Special rollers were used to prevent any air intrusions. Each layer can give a thickness of an average value of (2.0 – 2.5 mm). To obtain several thicknesses of GFRP laminates, the previous steps were repeated several times. Figure 1 shows the shape of used discrete glass fibres, woven roving layers, and shopped mates. The tensile properties of the

shopped mate and the woven roving was according to manufacturer data sheet and was following ASTM (D4595) [26] . Table 1 shows the mechanical properties of used fabrics.

| Discrete Glass Fiber | Woven Roving Sample | Shopped Mate Sample |

Fig. 1: Typical Components for GFRP Laminate

Table 1: Mechanical Properties of Shopped Mate & Woven Roving

Property	Shopped Mate	Woven Roving
Tensile Strength (N/m)	180.50	25660
Secant Stiffness up to 3% (N/m)	71.82	847500
Offset Tensile Modulus (N/m)	25038.571	1196333
Energy to Break (J/m²)	3.202	401.971
Strain Break (%)	3.963	3.146

2.3. Resins

Polyester resin with medium reactivity and medium viscosity was used as a binder for fibres and was also used to paste GFRP to steel surfaces as per manufacturer recommendations. The tensile property of used polyester is issued by the data sheet from the manufacture, as shown in Table 2.
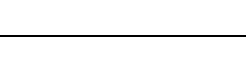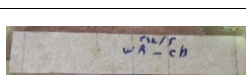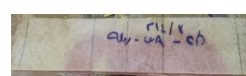
Table 2: Mechanical Properties of Polyester
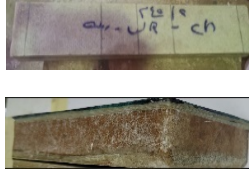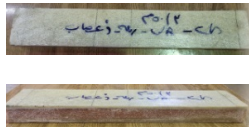
Property	Polyester
Tensile Strength (MPa)	75
Elongation at Break (%)	3.5
Tensile Modulus (MPa)	3700
Flexure Strength (MPa)	125
Flexure Modulus (MPa)	3800

2.4. Specimens Preparation

Thirteen specimens of pure steel, twenty-four specimens of GFRP, and four composite specimens of combination between both mater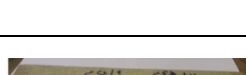ials were prepared for examination. Table 3 shows summary of the tested specimens. For all specimens examined in flexure, the beams were test with a total length of 500 mm with a gauge length of 450 mm. All beams had a width of 100 mm while the thicknesses were variable and shown in Table 3. For tensile specimens, the coupons configuration was also mentioned in the same table.

Table 3: Description of Examined Specimens for Flexure and Tensile Tests

Type	Specimen ID	Test	No. of Specimens	Description	Photo
Steel	S1.5	Tension	3	Coupon of thickness1.5mm	
	S7	Flexure	2	Beam of thickness 7 mm	
	S14	Flexure	2	Beam of thickness 14 mm	
	S28	Flexure	2	Beam of thickness 28 mm	
	RST50-2	Flexure	2	*Ribbed beam of the upper and lower skin plate thickness (2 mm) and web (3mm)	
	RST50-3	Flexure	2	Ribbed beam of the upper and lower skin plate thickness (3 mm) and web (4mm)	
GFRP	GF2.5	Tension	2	L = 30cm, W = 2.5cm and Th.= 2.5 mm	
	GF7	Tension	2	L = 30cm, W = 2.5cm and Th.= 7.0 mm	
	GF14	Flexure/ Tension	4	Glass fiber beam of thickness 14 mm	
	GF28	Flexure/ Tension	4	Glass fiber beam of thickness 28 mm	
	GF45	Flexure/ Tension	4	Glass fiber beam of thickness 45 mm	
	GFS14	Flexure	2	Sandwich beam (Th. 14 mm) Upper and lower GFRP layers (4.5 mm) – infilled cemented sand layer (5.0 mm)	

Type	Specimen ID	Test	No. of Specimens	Description	Photo
Compo site	GFS28	Flexure	2	Sandwich beam (Th. 28 mm) Upper and lower GFRP layers (9.0 mm) – infilled cemented sand layer (10 mm)	
	GFS45	Flexure	2	Sandwich beam (Th. 45 mm) Upper and lower GFRP layers (15 mm) – infilled cemented sand layer (15 mm)	
	RGFS50	Flexure	2	** Ribbed beam of upper, lower, and web plates of (Th.= 4 mm) with infilled cemented sand layer	
	S7-GF2.5	Flexure	2	Steel beam of Th. 7.0 mm + attached GFRP (Th. = 2.5 mm) - both sides	
	S7-GF7	Flexure	2	Steel beam of Th. 7.0 mm + attached GFRP (Th. = 7.0 mm) – both sides	

* For the steel beams, ripped beams was formed as follow: two outer flanges were connected by means of vertical webs, where all connections were applied using weld. The in-between space was left empty.

**For GFRP beams, the fabrication was done by extending and merging some of GFRP layers from both flanges to the web. The in-between space was filled with cemented sand incorporated discrete fibres. Polyester resin was used for binding. Strands of fibres played a role in enhancing the connection between upper and lower flanges.

3. Experimental Program

3.1. Flexure Test Setup
The flexure test was performed according to ASTM-D790 [27]. A four-point loading test was followed in this research to estimate the flexural behaviour of the examined plates. Figure 2 shows the test setup, where the applied load was developed using a manual hydraulic jack of 25 Ton capacity. The applied load was measured by an available load cell with a maximum capacity of 5 Tons. Three linear variable displacement transducers

(LVDTs) were used to measure the deflection. Two transducers were placed at supports while the third was kept at the middle of the specimen. The strain was measured using an available strain gauge, 30 mm for steel specimens and 60 mm for GFRP specimens. one strain gage was pasted to the middle of the soffit layer of each specimen. The specimens were loaded until complete failure or till reaching the maximum capacity of the load cell. According to ASTM D790 [27], the flexure stress, the strain and the tangent modulus of elasticity can be determined as follows:

$$\sigma = \frac{3PL}{2bd^2} \tag{1}$$

$$\xi = \frac{6Dd}{L^2} \tag{2}$$

$$E = \frac{L^3 m}{4bd^3} \tag{3}$$

Moreover, the displacement ductility index (μ) was also calculated as the ratio of ultimate displacement to the yield displacement [28] and can be written as follows:

$$\mu = \Delta u \, / \, \Delta y \tag{4}$$

Where:

    σ: Stress of the outer fibres at mid-span (MPa)
    P: Load at a given point in Load Deflection Curve (N)
    L: Support Span (mm)
    b: Width of the beam assessed (mm)
    d: Thickness of the tested beam (mm)
    ξ: Strain at the outer surface (mm/mm)
    D: Maximum deflection (mm)
    E: Tangent modulus of elasticity (MPa)
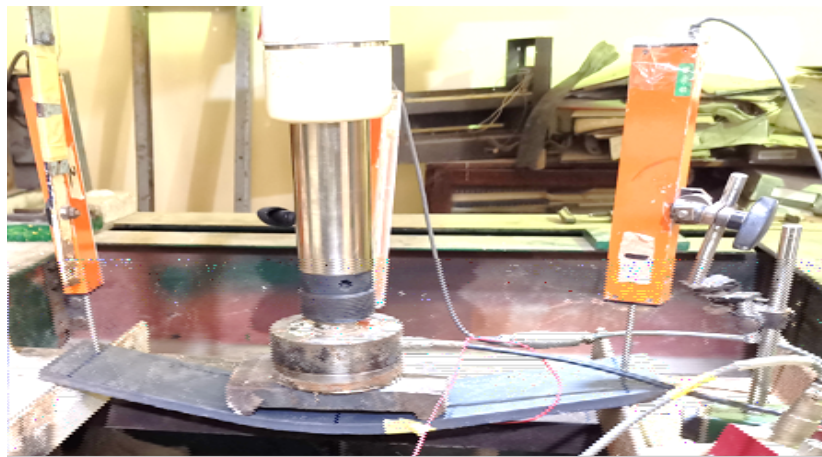   m: Slope of tangent to the initial straight-line portion of the Load-Deflection curve.

Fig. 2: Flexure Test Configuration

3.2. Tensile Test Setup

The tensile test was performed according to ASTM-D3039 [29]. All specimens were prepared with a total length of 500 mm, a width of 50 mm, and variable thicknesses. The specimens were mounted in the grips of a mechanical testing machine. The ultimate tearing forces along with the mode of failure were recorded. The ultimate strength of the material could be determined by directly dividing the maximum force at failure by the cross-sectional area of specimens. Also, the strain was measured using an available strain gauge, 30 mm for steel specimens and 60 mm for GFRP specimens. one strain gage was pasted in the half of soffit of each sample. Figure 3 shows the tensile test setup.

Fig. 3: Tensile Test Setup

4. Results and Discussion

4.1. Flexure Test

Load-deflection curves and Stress-Strain curves were expressed as an average value for the tested specimens. Figure 4 shows load-deflection curves for all specimens. Figure 5 shows the corresponding Stress-Strain plots for the same specimens. It was noted that as the thickness increased the load carrying capacity also increased. For steel specimens, the ultimate load was increased for S14 and S28, almost 3, and 6.7 times that of S7, respectively. The ductility index was increased by increasing the specimens' thickness; μ was 4.2, 5.5, and 6.5 for S7, S14, and S28, respectively. Figure 6 depicts the ductility index for steel specimens. For S14 and S28 the deflection decreased by 15% and 25%, respectively at ultimate load compared to S7. The deflections were 30% and 79%, respectively, at the end of the elastic zone compared to S7. As per ribbed specimens, better performance was achieved for RST50-2 and RST50-3 during loading. Unfortunately, the load stopped as per the capacity of the loading cell. It is, however, observed that for any loading level, smaller deformation was achieved. This could be attributed to the high equivalent of Young's modulus in the elastic zone region.

GFRP exhibited good loading performance. The loading capacity of some specimens achieved as much load as steel sections of less thickness. For example, GF45, the biggest GFRP thickness, reached an ultimate load of approximately 99% of S28 and twice that of S14. Also, GF14, of the least GFRP thickness, reached almost 88%, 33%, and 10% of the

ultimate load of steel specimens S7, S14, and S28, respectively. It is however, brittle behaviour was achieved for all specimens. As the specimens reached their ultimate loading capacity, the specimens showed sudden failure. This could also be solved by setting strain limits for GFRP specimens as an attempt to prevent unexpected failure criteria.

Focusing on GFRP specimens, GF14 reached an ultimate load capacity of 5.4 KN with a corresponding deflection of 37.5 mm and an ultimate strain of 0.9%. GF28 reached 6.8 times the load-carrying capacity of GF14 with a maximum deflection of 29 mm. It was noted that the strain gauge was cut to 20 KN with a strain of 1.2% due to the tearing of fibres near the gauge. For GF45, the loading stopped at the ultimate load capacity of the load cell. To optimize the use of GFRP, the same thicknesses were repeated but after incorporating a cemented sand layer as infilled material in between two GFRP laminates.

GFS14 had the same loading behaviour as GF14 and reached an ultimate load of 7.4 KN, the monitored strain reached 1.9%. As the thickness increased, sand started to escape from the sides leading to acceleration of the failure of specimens. This could be depicted through an overall decrement in the section modulus. GFS28 achieved 72% of the ultimate load capacity of GF28. Whereas the ultimate deflections were the same. For ribbed GFRP specimens incorporated sand like RGFS50; the test was stopped as reaching the ultimate load capacity of the load cell, however, the loading trend showed the best performance through the elastic zone. It was also thought that confining the sand by additional wrapping could work on better loading performance. The results indicated the importance of using such a promising material to withstand bending stresses compared to steel. Figure 6 shows a summary of pure specimens' loading behaviour with insight into the ductility index for all specimens. The elastic modulus was calculated for all beams by calculating the slope of the curve in the elastic zone at 3% strain for all specimens and shown in Tables 4 and 5. The obtained results will be considered for further implementation when designing of large-scale gates.
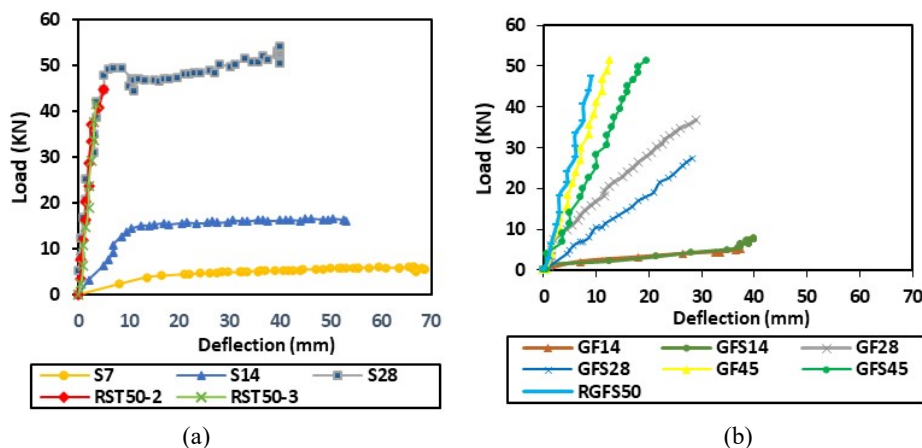

(a)   (b)

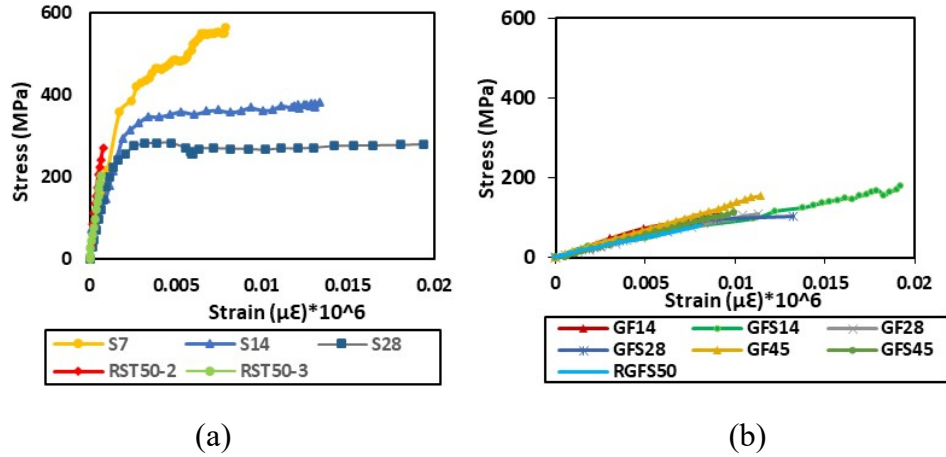Fig. 4: Load-Deflection Curves for a) Steel and b) GFRP Specimens
From Flexure Test

(a)   (b)

Fig. 5: a) Stress- Strain Curves for a) Steel and b) GFRP Specimens
From Flexure Text

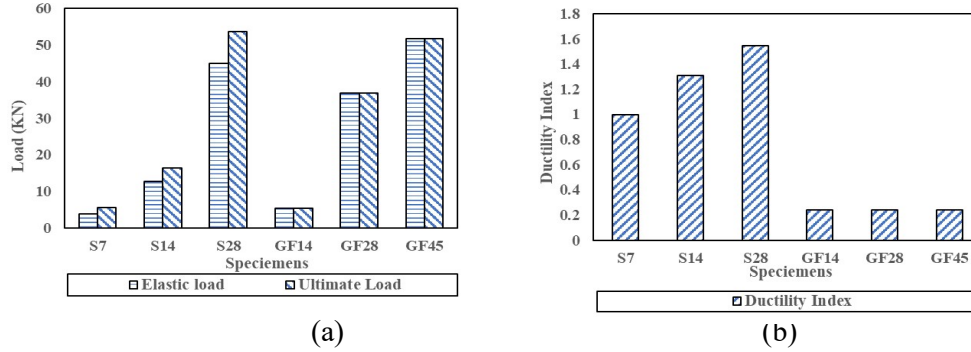(a)   (b)

Fig. 6: a) Summary of Loading Results with Insight to b) Ductility Index for
Steel and GFRP Specimens from Flexure Test

Table 4: Equivalent elastic modulus for all steel Specimens

Specimen	S7	S14	S28	RST50-2	RST50-3
E (MPa)	2.06E+05	1.96E+05	1.98E+05	3.11E+05	3.17E+05

Table 5: Equivalent elastic modulus for all GFRP Specimens

Specimen	GF14	GF28	GF45	GFS14	GFS28	GFS45	RGFS50
E (MPa)	19329.69	11456.37	17578.7	8100.86	9517.682	10764.39	9859.15

For comparison purposes, the specimens of thickness 28 mm were selected and put into a
glance. The load-carrying capacity, and achieved deflection for S28, GF28, and GFS28
were presented in Figure 7. The steel material can sustain a maximum load of up to 1.4 and
1.6 times that of GF28 and GFS28, respectively. The maximum deflection for S28 was 1.37
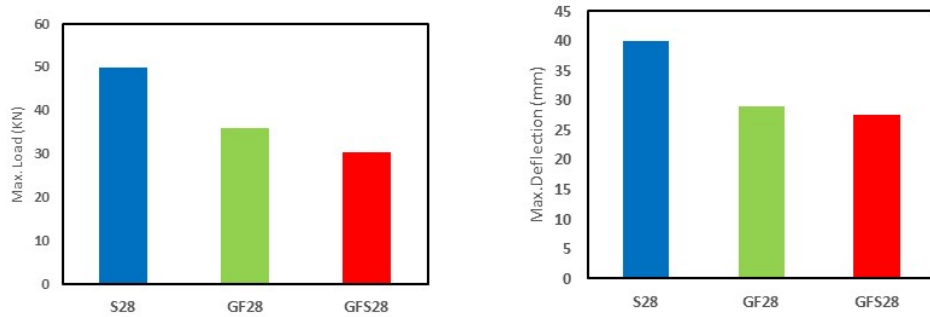and 1.45 times that of GF28 and GFS28, respectively.

Fig. 7: Maximum Obtained Load and Deflection for Specimens of Same Thickness

The research also aimed to check the strengthening of steel plates GFRP sheets. Typical steel plates of thickness 7 mm were strengthened with laminates of GFRP of 2.5 mm, and 7 mm, pasted to the soffit of the steel specimens. For these composite specimens, load-deflection as well as stress-strain curves have been introduced in Figure 8. For S7-GF2.5 and S7-GF7, the ultimate capacity was increased by 40% and 80 %, respectively, compared with S7. Figure 9 represents a comparison of the three composite specimens in graph form.
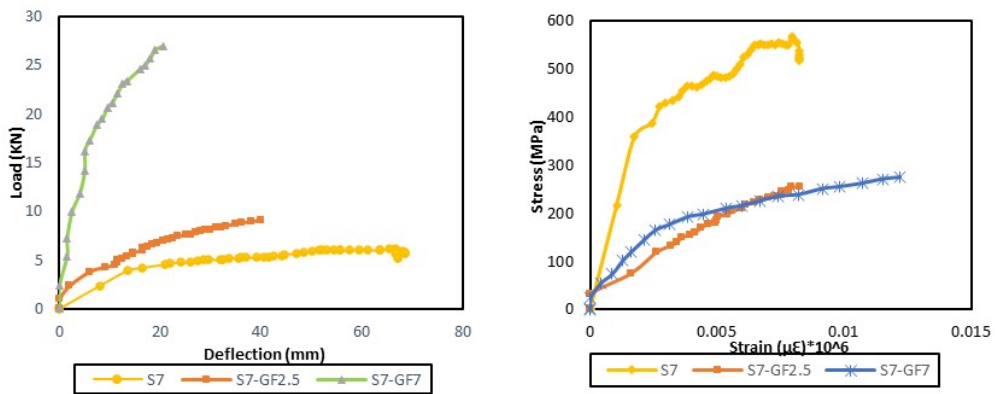

Fig. 8: Load-Deflection and Stress-Strain Relationships for Composite Sections
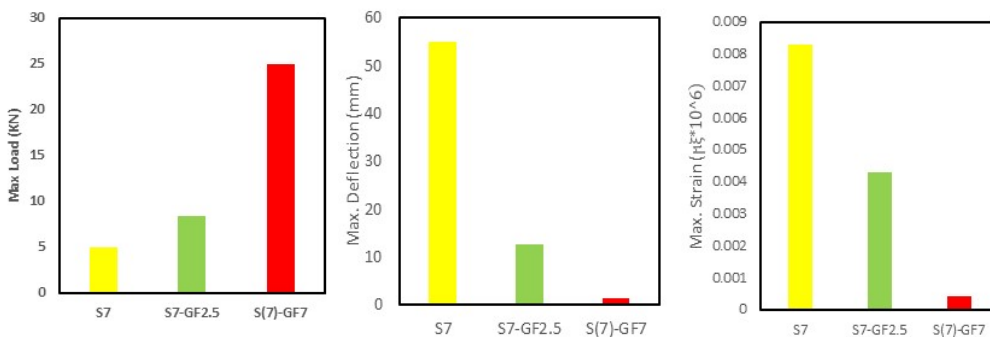from Flexure Test

Fig. 9: Behavior of Three Configurations at 7mm Thickness

4.2. Flexure Failure Modes

The following section represents the description of the captured failure modes for tested specimens. For the pure steel plates, deflection increased by loading then the yielding of steel occurred. The test ended up with signs of plastic deformations. The thinner the specimens the larger the deflection occurred. For ripped steel specimens, deformations showed extremely lesser values until reaching the ultimate capacity of the loading cell. For RS50-2, local buckling was monitored before reaching global failure. This, in turn, reflects the important need to examine the stability of every single component in the ribbed mechanism. For RS50-3, the specimens are more rigid. The experimental results showed that maximum elastic deflection reached 5 mm at the maximum load capacity of the load cell. This deflection has been released with the removal of loading leaving no plastic deformation among specimens.

For pure GFRP specimens, tearing in the outer fibres subjected to tension occurred. As thickness got thicker, the interfacial debonding affected the failure mechanism significantly. For GF14 and GF28, the concentration of stresses under the location of applied point loads led to tearing at these locations. For GF45, interfacial debonding occurred and slight sliding was captured in between GFRP layers. This could lead to the necessity of bolting using FRP filaments in thick samples.

For GFRP beams stuffed with sand specimens, for thin layers like the case of GF14, the sand layer worked in reducing the overall cost while achieving the same loading capacity and mode of failure. Tearing of GFRP layers was achieved. For thicker layers of sand like in the case of GF28 and GF45, the modes of failure occurred by crumbling and escaping of sand layer. This could lead to further enhancement of making additional wrapping of the sand and making some confinement to prevent interfacial debonding between sand and GFRP layers. No tearing in GFRP layers was observed. For the ribbed specimen, RGFS50, the mode of failure started with interfacial debonding between the sand layer and GFRP. Crumbling in the sand also occurred. It was also noted that specimens that included sand exhibited larger deformations than their corresponding thicknesses with no sand.

For composite specimens, the interfacial debonding failure occurred in between the steel and GFRP layers. Elastic deformation for steel plates whereas plastic deformation occurred in GFRP laminates. It was noted that as GFRP layer thickness increased, the plate became more rigid, but the overall section ductility decreased. Figures 10, 11, and 12 show the mode of failure among examined steel, GFRP, and composite specimens, respectively.

S7   S14   S28
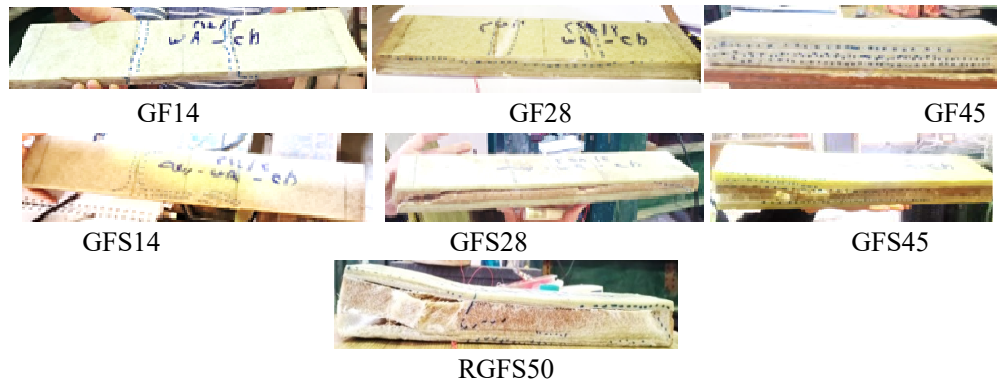
RS50-2   RS50-3

Figure 10: Deformations for Steel Beams

GF14   GF28   GF45

GFS14   GFS28   GFS45

RGFS50
Fig. 11: Mode of Failure for GFRP

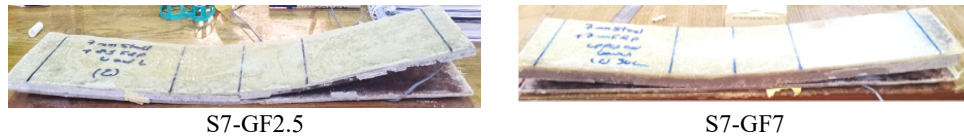S7-GF2.5   S7-GF7
Fig. 12: Modes of Failure of Composite Specimens

4.3. Tensile Test Results

Figure 13 represents a comparison between the maximum tensile forces at failure for GFRP specimens as well as the control steel specimen with 1.5mm thickness. It was noted that for all specimens' rupture was the dominant mode of failure. For GF45, rapture started just near the grips with sudden tearing to the whole section. For GF28, the tearing started from the outer to inner layers and debonding occurred in the middle of specimens. For GF14, tearing happened to the whole section at once. for small specimens, GF7, and GF2.5, the tearing started at notch location. Axial strength was then calculated as an average for similar specimens' configurations. For all specimens, the average tensile strength was a narrow range except for GF14, where the axial strength reached almost 1.57 times the average values for the rest of the specimens. This could be concerned with further design aspects. Figure 14 shows the average tensile strength for GFRP specimens with a trendline for the average value. Figure 15 shows the failure modes for all test specimens.
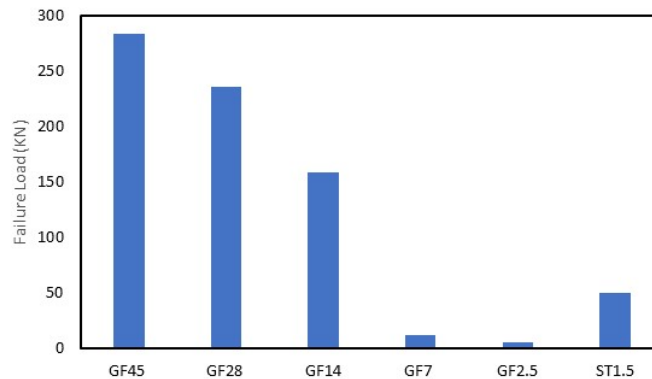

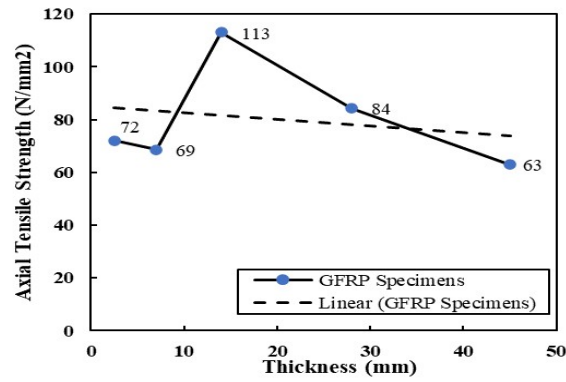Fig. 13: Maximum Failure Load for all Specimens

Fig. 14: Average axial strength for GFRP specimens

Prism – GF45	Prism – GF28	Prism – GF14	Prism – GF7	Coupon – GF1.5	Coupon – S1.5
(Tearing)	(Tearing)	(Tearing)	(Tearing)	(Tearing)	(Yielding)
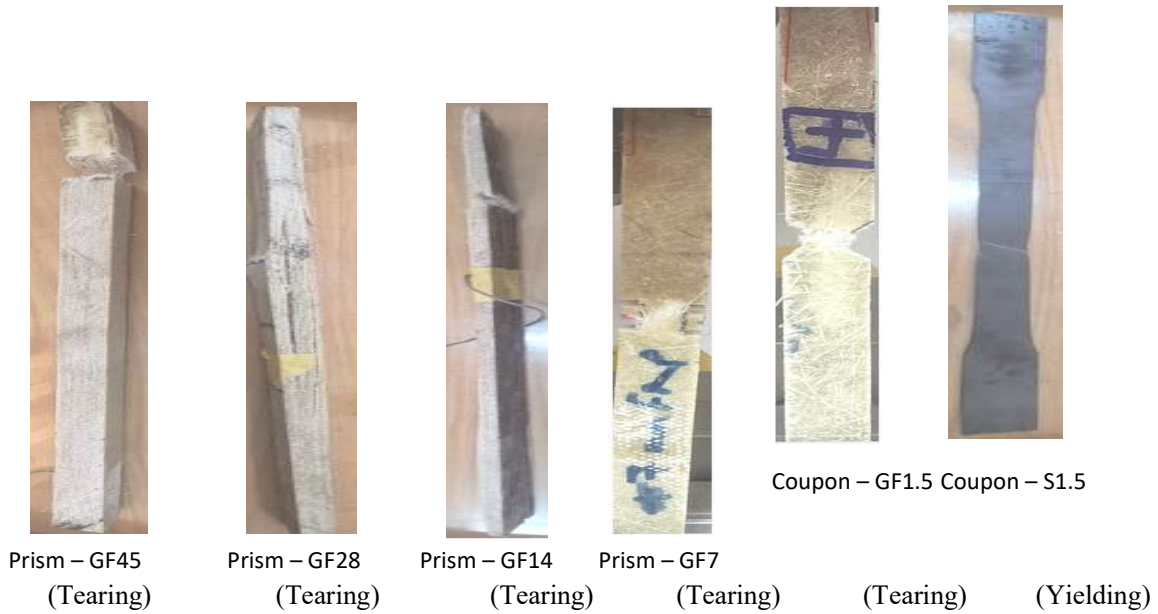
Fig. 15: Modes of Failure for Specimens Failed in Tension

5. Numerical Application

The nonlinear finite element software ABAQUS [30] was employed for numerical simulation of the two types of the gates: steel gate with thickness 14 mm (ST14), and pure GFRP gates of thickness 29 mm (GF29) and 45 mm (GF45). The gates have a typical dimension of (1000 x 1000 mm). The properties of the used materials were taken from the carried experimental work. Deformable 3D - 8 nodes with reduced integration solid part was used to simulate the gates. This element can be used to improve the calculation efficiency, and to obtain more accurate stress fields and displacements.

5.1. Model Description

Nonlinear material was utilized in defining the material of gates. For GFRP gates, the formation of a given thickness required applying several layers of GFRP laminates practically. The properties were defined as per the experimental data. In ABAQUS, the linear elastic portion of the material stress-strain curve is defined by the modulus of elasticity. However, the non-linear portion of the material requires definition of the real stress-plastic strain behaviour. For the linear portion of analysis, the steel gate was simulated by the following: yielding stress of 360 MPa, modulus of elasticity of 1.96E+05 MPa and Poisson's ratio of 0.3. For GFRP gates the ultimate stress was 160 MPa, and equivalent elastic modulus was 17578.7 MPa for GF45 and 11456.37 MPa for GF29. For non-linear portion of the steel material, the ultimate stress was 554 MPa at a corresponding plastic strain 0.268 (mm/mm). A fine mesh was used to provide accuracy at both elastic and plastic behaviours. The gates were divided into mesh of size (25 x 25 mm) for in-plane discretization whereas the thickness was divided into 2, 4 and 5 elements for ST14, GF29, and GF45, respectively. Figure 16 shows the finite element models for the three gates. The gates were restrained from translation in all directions along the two vertical edges of the gates. The gates were subjected to triangular hydrostatic pressure equivalent to the gate height (1 m), as shown in Figure 17.

(a)   (b)   (c)

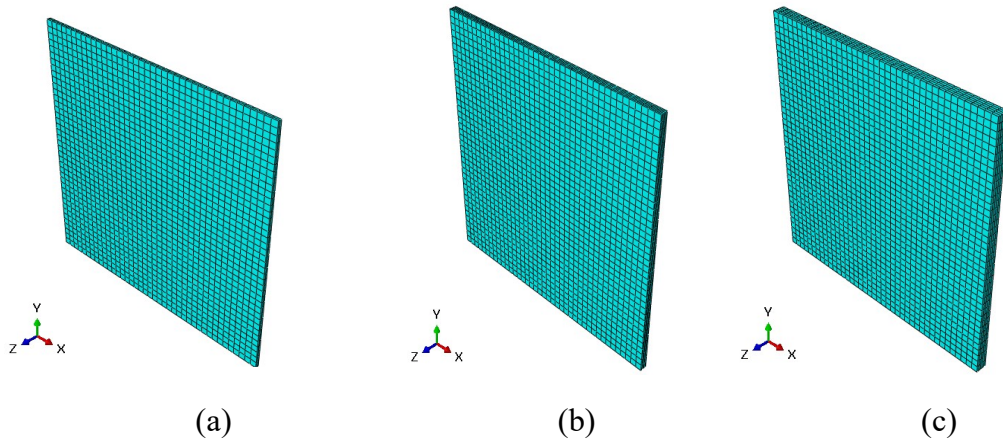Fig. 16: Mesh configuration; (a) ST14, (b) GF14, and (c) GF45 Gates

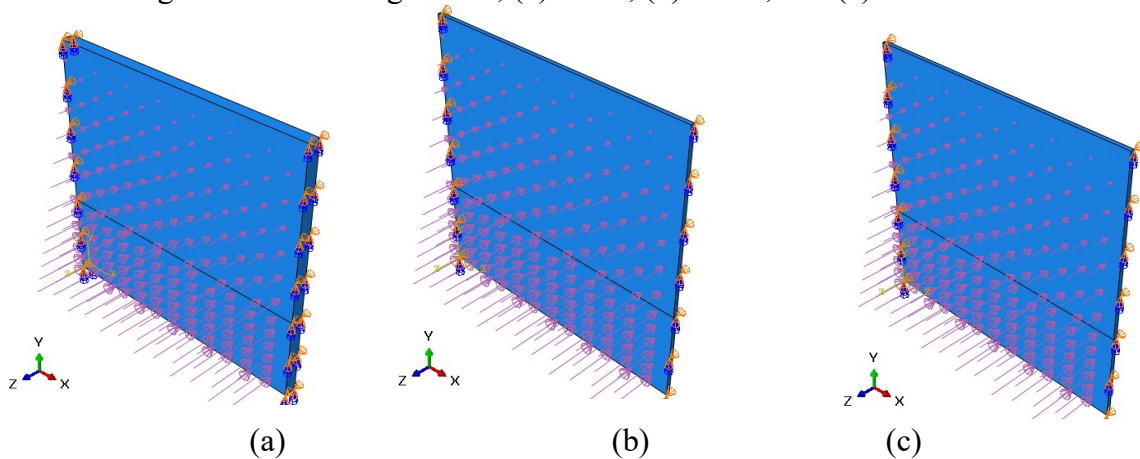(a)   (b)   (c)

Fig. 17: Load Configuration & Boundary Condition; (a) ST14, (b) GF14, and (c) GF45 Gates

5.2. Numerical Results

The results of the numerical simulations are explored in this section. Comparisons of results in terms of maximum displacements, stresses, and strains were conducted. Figures (18 – 20) show the obtained stress, displacement, and strains for the three gates.
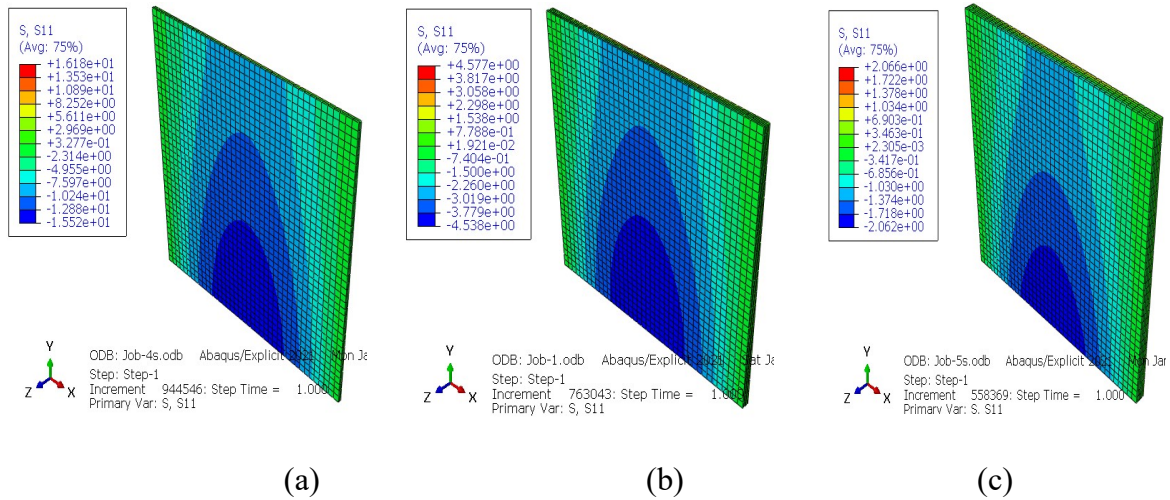

(a)   (b)   (c)

Fig. 18: Horizontal Stress Distribution for (a) ST14, (b) GF29, and (c) GF45

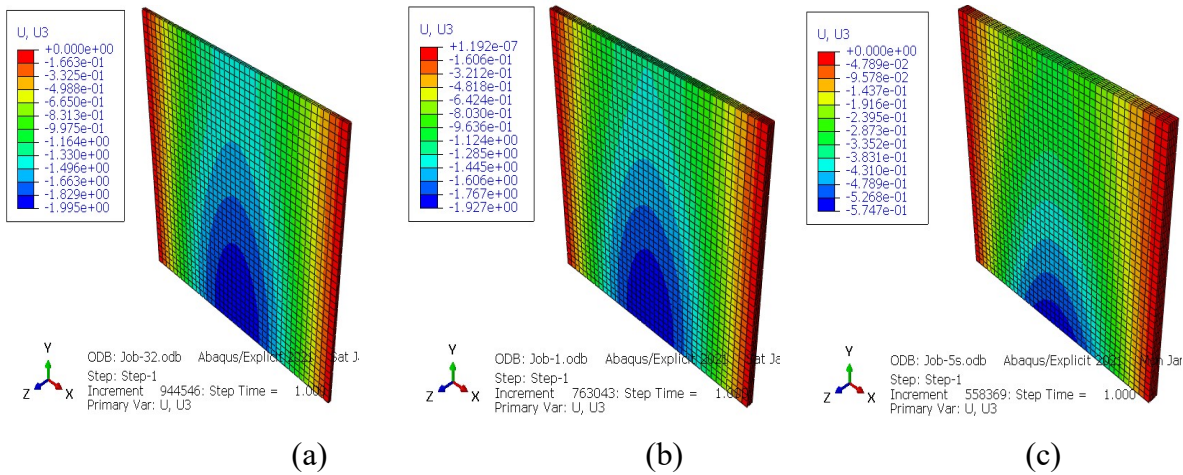(a)   (b)   (c)

Fig. 19: Horizontal Displacement Contours for (a) ST14, (b) GF29, and (c) GF45

Synthetically, the steel gate was solved and kept for control. After several trials, GF29 was found of equal flexural stiffness as the steel gate. GF29 gave the same deformation under the same load as ST14. It is however, found that the strain in the GF29 was much greater than ST14. Thus, another trail was done to reduce the strain values to almost half the values obtained in GF29. This could help in maintaining the creep that might occur in the gate. Thus, GF45 was assumed to be a good choice for practical implementation. For GF45, a decrease in both displacement and stresses in the horizontal direction of 71, and 87% compared to ST14. As a result, GFRP showed a promising tool to replace hydraulic steel gates of small dimensions.

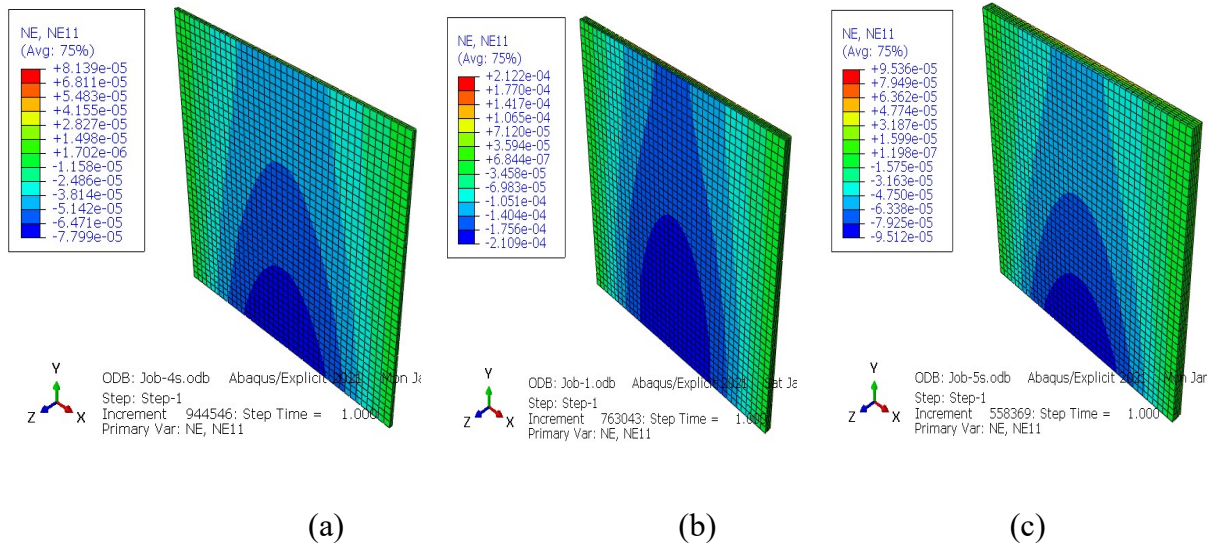(a)   (b)   (c)

Fig. 20: Horizontal Strain for (a) ST14, (b) GF29, and (c) GF45

6. Conclusions

The current research is considered an attempt to use GFRP as suitable alternative for small-size steel gates. Depending on the performed Laboratory and numerical simulations, the following were concluded:

- GFRP showed good results to sustain flexure forces compared to steel with probability of low maintenance costs.
- GFRP sections can achieve steel ultimate capacity with almost half their thicknesses, whereas the ductility of steel specimens was much better.
- The ribbed steel system has good behavior regarding tested plates. By comparing the behavior of S28 and RST50-2, the two specimens sustain the same load, but the RST50-2 specimen gave strain and defection 50% and 85% lower than S28 with almost 50% reduction in mass.
- For pure GFRP specimens subjected to flexure, smaller thicknesses were subjected to tearing of fibers whereas thicker thicknesses were subjected to interfacial debonding failure. It is recommended to have additional fiber bolting or connecting filaments between outer surfaces.
- For GFRP-incorporated sand, it was noticed initial failure due to the escaping of sand from both sides of laminates; interfacial debonding was the common mode of failure. However, their flexure behavior was the same as pure GFRP samples of the same thickness till failure. Recommendations for additional wrapping should be considered.
- For ribbed GFRP specimens, the best flexure performance was achieved.
- For composite steel and GFRP specimens, increasing the thickness of the strengthened GFRP layer led to an increase in the load-carrying capacity significantly. S7-GF7 achieved 80% more load than S7 whereas, the defection decreased by 97% compared to S7.

- Numerical results for small size gates showed good aggrement with the experimental work. GFRP gates of almost doube the steel thickness was suffecient to bear same loading capacity. Precautions have to be made to maintain creep thus thicker GFRP gate was selected.
- Due to the brittleness of GFRP, recommendations to set limitation criteria for strain should be performed.

References

[1]   O. P. C. Series and M. Science, "*The Efficiency of Steel Material as Buildings Construction The Efficiency of Steel Material as Buildings Construction*," 2020, doi: 10.1088/1757-899X/879/1/012148.

[2]   L. Dai and X. He, "*Experimental Study on Tensile Properties of GFRP Bars Embedded in Concrete Beams with Working Cracks*," MATEC Web Conf., vol. 88, pp. 0–5, 2016, doi: 10.1051/matecconf/20178802005.

[3]   M. S. Travis Adams, "*FATIGUE OF HYDRAULIC STEEL STRUCTURES – PIANC WG 189*," pp. 1–2, 2018.

[4]   K. Murakami, T. Wakahara, I. Fukunaga, and H. Sakai, "*Design of hydraulic performance*," JSAE Rev., vol. 18, no. 3, pp. 306–309, 1997, doi: 10.1016/S0389-4304(97)00006-4.

[5]   C. Baumgart, T. Halle, C. Weigelt, L. Krüger, and C. G. Aneziris, "Effect of honeycomb cell geometry on compressive properties: Finite element analysis and experimental verification," Sci. Technol. Mater., vol. 30, no. 1, pp. 35–42, 2018, doi: 10.1016/j.stmat.2018.02.001.

[6]   T. Tomiyama and I. Nishizaki, "Applicability of fiber reinforced plastics to hydraulic gates," Compos. Civ. Eng. CICE 2006, no. Cice, pp. 453–456, 2020.

[7]   P. Walunj, P. Thokal, K. Bidwai, and T. Jagtap, "Design & Analysis of Radial Dam Gate Using Glass Fibers," vol. 6, no. 4, pp. 318–321, 2019.

[8]   P. V. Vijay, P. R. Soti, H. V. S. GangaRao, R. G. Lampo, and J. D. Clarkson, "Design and evaluation of an integrated FRP composite wicket gate," Compos. Struct., vol. 145, pp. 149–161, 2016, doi: 10.1016/j.compstruct.2016.01.093.

[9]   J. C. Trovillion, J. P. Ryan, and J. W. Harper, "*FIBER REINFORCED POLYMER COMPOSITE IMPLEMENTATION IN by*," pp. 1–10, 2018.

[10]   R. Sonnenschein, K. Gajdosova, and I. Holly, "*FRP Composites and their Using in the Construction of Bridges,*" Procedia Eng., vol. 161, pp. 477–482, 2016, doi: 10.1016/j.proeng.2016.08.665.

[11]   C. G. M and N. Bhanuprakash, "*a Review on Mechanical Properties of Gfrp With Different Filler Materials,*" Int. Res. J. Eng. Technol., vol. 4, no. 5, pp. 275–278, 2017.

[12]   M. M. Önal, "*Strengthening reinforced concrete beams with CFRP and GFRP*," Adv. Mater. Sci. Eng., vol. 2014, 2014, doi: 10.1155/2014/967964.

[13]   M. M. Majed, M. Tavakkolizadeh, and A. A. Allawi, "*Analytical study on torsional behavior of concrete beams strengthened with fiber reinforced polymer laminates using softened truss model*," Adv. Struct. Eng., vol. 24, no. 8, pp. 1642–1654, 2021, doi: 10.1177/1369433220981693.

[14]   A. Landesmann, C. A. Seruti, and E. D. M. Batista, "*Mechanical properties of glass fiber reinforced polymers members for structural applications,*" Mater. Res., vol. 18, no. 6, pp. 1372–1383, 2015, doi: 10.1590/1516-1439.044615.

[15]   R. Raval and U. Dave, "*Behavior of GFRP wrapped RC columns of different shape*s," Procedia Eng., vol. 51, no. NUiCONE 2012, pp. 240–249, 2013, doi:

10.1016/j.proeng.2013.01.033.

[16]   P. Pv, "*Analysis of Cold-Formed Steel Built-up Closed Sections Strengthened with GFRP*," pp. 1–14, 2022.

[17]   J. L. Abbas and A. A. Allawi, "*Experimental and Numerical Investigations of Composite Concrete–Steel Plate Shear Walls Subjected to Axial Load*," Civ. Eng. J., vol. 5, no. 11, pp. 2402–2422, 2019, doi: 10.28991/cej-2019-03091420.

[18]   T. A. Kinjawadekar, S. Patil, and G. Nayak, "*A Critical Review on Glass Fiber-Reinforced Polymer Bars as Reinforcement in Flexural Members*," J. Inst. Eng. Ser. A, vol. 104, no. 2, pp. 501–516, 2023, doi: 10.1007/s40030-023-00729-6.

[19]   A. Nazir, A. Bin Arshad, S. C. Lin, and J. Y. Jeng, "*Mechanical Performance of Lightweight-Designed Honeycomb Structures Fabricated Using Multijet Fusion Additive Manufacturing Technology*," 3D Print. Addit. Manuf., vol. 9, no. 4, pp. 311–325, 2022, doi: 10.1089/3dp.2021.0004.

[20]   S. T. Method, "*Standard Test Methods for Tensile, Compressive, and Flexural Creep and CreepRupture of Plastics*," vol. 08, no. Reapproved 1989, pp. 3–4, 2000.

[21]   M. F. Sá, A. M. Gomes, J. R. Correia, and N. Silvestre, "*Creep behavior of pultruded GFRP elements - Part 1: Literature review and experimental study*," Compos. Struct., vol. 93, no. 10, pp. 2450–2459, 2011, doi: 10.1016/j.compstruct.2011.04.013.

[22]   S. Loni, I. Stefanou, and P. S. Valvo, "*Experimental study on the creep behavior of GFRP pultruded beams*," XXI Congr. AIMETA (Associazione Ital. di Mecc. Teor. e Appl., pp. 1–10, 2013.

[23]   S. Beddu, A. Syamsir, Z. A. M. Ishak, Z. M. Yusof, N. S. Hudi, and S. Nabihah, "*Creep behavior of glass fibre reinforced polymer structures in crossarms transmission line towers,*" AIP Conf. Proc., vol. 2031, 2018, doi: 10.1063/1.5066995.

[24]   E. Code and O. F. Practice, "*Egyptian Code of Practice 'Allowable Stress Design,'*" no. 279, 2001.

[25]   C. Lu, Y. Yang, and L. He, "Mechanical and durability properties of GFRP bars exposed to aggressive solution environments," Sci. Eng. Compos. Mater., vol. 28, no. 1, pp. 11–23, 2021, doi: 10.1515/secm-2021-0002.

[26]   ASTM D4595, "*Standard Test Method for Tensile Properties of Geotextiles by the Wide-Width Strip*," Astm, vol. i, no. Reapproved, pp. 1–13, 2015, doi: 10.1520/D4595-17.Copyright.

[27]   ASTM D790, "*Standard Test Methods for Flexural Properties of Unreinforced and Reinforced Plastics and Electrical Insulating Materials. D790*," Annu. B. ASTM Stand., vol. i, pp. 1–12, 2002, doi: 10.1520/D0790-17.2.

[28]   J. H. Ling, Y. Lim, and E. Jusli, "*Methods to Determine Ductility of Structural Members: A Review*," J. Civ. Eng. Forum, pp. 181–194, May 2023, doi: 10.22146/jcef.6631.

[29]   ASTM D3039, "*Astm D3039/D3039M*," Annu. B. ASTM Stand., pp. 1–13, 2014, doi: 10.1520/D3039.

[30]   Simulia, "*ABAQUS/CAE User's Guide*," Dassault Systèmes Simulia Corp., p. 14, 2014, [Online]. Available: www.3ds.com/simulia.